Circum-Arctic Sediment PROvenance Database (CASPROD): A database of mineralogy and geochemistry for the Circum-Arctic surface sediments

Zhengquan Yao[1,2*], Han Feng[1], Ruediger Stein[3,4,5], Yanguang Liu[1,2], Xuefa Shi[1,2], YuriVasilenko[6], Seung-Il Nam[7], Linsen Dong[1,2], Fengdeng Shi[1,2], Kunshan Wang[1,2], Zhihua Chen[1,2], Shuqing Qiao[1,2], Qiuling Li[1], Song Zhao[1], Xinyue Pei[1], Huiyu Guo[1], Yaru Liu[1]

[1] Key Laboratory of Marine Geology and Metallogeny, Shandong Key Laboratory of Deep-Sea Mineral Resources Development, First Institute of Oceanography, Ministry of Natural Resources, 266061 Qingdao, China

[2] Laboratory for Marine Geology, Qingdao Marine Science and Technology Center, 266237 Qingdao, China

[3] Faculty of Geosciences, University of Bremen, 28359 Bremen, Germany

[4] Frontiers Science Center for Deep Ocean Multispheres and Earth System, Key Laboratory of Marine Chemistry Theory and Technology, Ocean University of China, 266100 Qingdao, China

[5] Alfred Wegener Institute, Helmholtz Centre for Polar and Marine Research, 27568 Bremerhaven, Germany

[6] V.I.Il'Ichev Pacific Oceanological Institute, Far East Branch of the Russian Academy of Sciences, 690041 Vladivostok, Russia

[7] Division of Glacial Environment Research, Korea Polar Research Institute, 21990 Incheon, Korea

***Correspondence:** Zhengquan Yao (yaozq@fio.org.cn)

Abstract

Arctic amplification is fundamentally reshaping the cryosphere, leading to accelerated sea-ice retreat, permafrost thaw, and intensified riverine discharge. These shifts collectively modify sediment source-to-sink dynamic processes in the Arctic

Ocean. While surface sediments in this semi-enclosed basin integrate complex signals from diverse Eurasian and North American source regions, disentangling these provenance signatures requires a robust, multi-proxy framework that has historically been hampered by fragmented, heterogeneous datasets. Here, we present CASPROD (Circum-Arctic Sediment PROvenance Database), a standardized and high-resolution mineralogical and geochemical synthesis of Arctic surface sediments. The dataset integrates multi-proxy records from a broad spatial network, comprising 4308 sampling stations, including bulk sediment Sr-Nd isotopes (n=175 stations), detrital zircon U-Pb ages (n=4671 grains from 21 key stations), clay mineral assemblages (n=1647 stations), and detrital mineral proportions (n=2465 stations). These integrated proxies provide cross-validated sediment provenance constraints: Sr-Nd isotopes discriminate between ancient cratonic shields and juvenile orogenic belts; detrital zircon geochronology yields diagnostic age spectra distinguishing Eurasian versus North American crustal affinities; and clay and detrital mineralogy reflects different circum-Arctic sediment provenances, lithologies and transport processes. By synthesizing these diverse datasets, CASPROD delineates robust pan-Arctic spatial provenance domains and transport pathways. This database thus provides a critical benchmark for reconstructing palaeoceanographic, glacial, and sedimentary dynamics over geological timescales. CASPROD is freely available online (https://doi.org/10.6084/m9.figshare.31926927; Yao et al., 2026) in multiple machine-readable formats (e.g., tabular tables, GIS shapefiles, and GEOTIFF).

1. Introduction

The Arctic region is currently warming at a rate approximately four times faster than the global average, a phenomenon known as Arctic amplification (Serreze and Barry, 2011; Rantanen et al., 2022). This rapid warming has accelerated a cascade of environmental responses, including sea-ice attrition and Greenland ice-sheet mass loss, enhanced permafrost thaw, and increased riverine discharge to the Arctic Ocean (White et al., 2007; The IMBIE, 2020; Stroeve and Notz, 2018; Natali et al., 2021). Beyond regional impacts on polar regions, these changes exert far-reaching influences on global climate system through atmospheric and oceanic teleconnections (Screen and Simmonds, 2010; Cohen et al., 2014; Henderson et al., 2021).

Crucially, climate-driven environmental changes have fundamentally reorganized sediment source-to-sink processes in the Arctic Ocean. Sea-ice retreat enhances the efficiency and spatial reach of ice-rafted sediment transport across Arctic basins (Darby, 2003; Eicken et al., 2005; Stein, 2008), while intensified precipitation and permafrost degradation due to thermokarst processes increase the fluvial flux of terrigenous materials (Holmes et al., 2002; Rusakov et al., 2025). In addition, the major circulation systems, including the Beaufort Gyre and the Transpolar Drift (Timmermans and Marshall, 2020), constantly modifies sediment dispersal pathways and redistribution patterns. Consequently, surface sediments act as a valuable archive, preserving integrated signals of sediment provenance, river input, sea-ice rafting, coastal erosion, and hydrodynamical conditions (for review see Stein, 2008; Myers and Darby, 2022).

Sediment inputs to the Arctic Ocean therefore form a complex spatial mosaic derived from geologically diverse circum-Arctic source regions, including the Eurasia, North America, Greenland, and the Canadian Arctic Archipelago (Gordeev, 2006; Martinez et al., 2009). While fluvial systems and coastal erosion supply primary materials, ice-rafted debris (IRD) and ocean currents facilitate basin-wide redistribution of sediments (Darby, 2003; Phillips and Grantz, 2001; Stein, 2008; McCave and Andrews, 2019). Accurate characterization of modern sediment provenance is thus a fundamental prerequisite for reconstructing paleoenvironmental history, including past source-to-sink process, ice-sheet dynamics, sea-ice history, and paleo-circulation patterns (e.g., Vogt, 1997; Philips and Grantz, 2001; Stein, 2008; Stein et al., 2010, 2025).

A range of provenance tracers, such as Sr-Nd isotopes, clay mineral assemblages, detrital (i.e., light and heavy) mineral compositions, detrital zircon U-Pb ages, major and minor elements, and Fe-oxide minerals, provide complementary constraints on sediment sources in the Arctic Ocean. Sr-Nd isotopes effectively distinguish sediments derived from juvenile orogenic belts and ancient Archean-Proterozoic cratons (Bazhenova et al., 2017; Maccali et al., 2018; Li et al., 2023), whereas detrital zircon U-Pb age spectra offer robust geochronological fingerprints that discriminate between North American and Eurasian basement affinities (Fedo et al., 2003; Feng et al., 2025). Clay mineral assemblages (e.g., Naidu and Mowatt, 1983; Stein et al., 1994, 2004; Wahsner et al., 1999; Thiry, 2000; Viscosi-Shirley et al., 2003a; Vogt and Knies, 2009; Saukel et al., 2010; Jang et al., 2023), detrital mineral assemblages (e.g., Vogt, 1996, 1997; Behrends, 1999; Stein, 2008; Wang et al., 2022), and major and minor elements (e.g., Schoster et al., 2000; Viscosi-Shirley et al., 2003a, 2003b) may reflect source-rock provenance, transport processes, and past varying climatic regimes. Fagel et al. (2014) have used mineral assemblages, trace element compositions and Nd and Pb isotope signatures to identify the detrital sediment provenance and to interpret changes in the relative contribution of the different source-areas in relationship to paleoenvironmental conditions. In addition, the chemical fingerprint of major and minor elements in specific Fe-oxide minerals, an approach developed by Darby and co-workers (Darby and Bischof, 1996; Darby, 2003; Darby et al., 2015), has been widely used to determine quite accurately sediment provenances in the Arctic Ocean and to reconstruct past sea-ice conditions (e.g., Darby, 2014; Tripati and Darby, 2018; Cofield and Darby, 2025).

Previous efforts have established several foundational databases for specific provenance proxies across the Arctic region. In a comprehensive synthesis study, Stein (2008) systematically compiled and mapped the spatial distributions of clay and detrital minerals throughout the Arctic Ocean, providing a critical reference framework (for data download and complete list of reference see Stein, 2026a, 2026b). This work characterized the composition of clay minerals (i.e., illite, chlorite, kaolinite and smectite) and selected detrital mineral assemblages and highlighted their significance for tracing sediment source regions and transport mechanisms of terrigenous materials (Stein, 2008). The mineralogical dataset was subsequently expanded in more recent compilations, notably by Myers and Darby (2022). In parallel, Fagel et al. (2014) and Maccali et al. (2018) synthesized a comprehensive Sr-Nd-Pb isotopic database for Arctic sediments. Despite these important contributions, a comprehensive and integrated provenance database that combines multiple proxies and incorporates newly published data remains lacking.

Here, we address this gap by compiling data from recent literature, with particular emphasis on newly generated datasets obtained from China-Russian joint investigations across the East Siberian Arctic shelf. The dataset integrates newly published Sr-Nd isotopic data (e.g., Li et al., 2023), clay mineral assemblages (e.g., Shi et al., 2018; Li et al., 2021; Jang et al., 2023), and detrital mineral compositions (e.g., Bazhenova, 2012; Dong et al., 2014; Gamboa et al., 2017; Andrews, 2019; Wang et al., 2024). In addition, the compilation is further expanded to include detrital zircon U-Pb geochronology data (Safonova et al., 2010; Wang et al., 2011; Feng et al., 2025). The database is designed with a structure that allows for continual updates, ensuring its long-term utility as a living resource for Arctic provenance research. Integrated analysis of these multi-proxy datasets enables the delineation of pan-Arctic spatial provenance patterns and provides new insights to the key processes governing modern source-to-sink pathways. Moreover, this database serves as a valuable benchmark for reconstructing sedimentary processes, glacial dynamics, and ocean circulation over geological time.

2. The CASPROD dataset

2.1 Regional subdivision of the Arctic Ocean: the Central Arctic Ocean and Marginal Seas

The CASPROD database integrates mineralogical and geochemical data covering the entire Arctic Ocean. To facilitate a systematic description and spatial analysis of these datasets, the Arctic Ocean is subdivided into two primary physiographic provinces, the Central Arctic Ocean and the Arctic Marginal Seas, following the classification scheme proposed by Jakobsson (2002) and Martens et al. (2021). Bathymetric constraints from the General Bathymetric Chart of the Oceans (GEBCO) were employed to delineate the shelf boundaries of these seas (Jakobsson, 2002). Within this framework, the Central Arctic Ocean encompasses the deep abyssal basins, specifically the Canada, Makarov, Amundsen, and Nansen Basins. The Arctic Marginal Seas are characterized by extensive continental shelves surrounding these basins, including the Beaufort, Chukchi, East Siberian, Laptev, Kara, and Barents Seas, as well as the shelf regions adjacent to the Canadian Arctic Archipelago (Figure 1, Table 1).

2.2 Lithological characteristics of the circum-Arctic continents

The mineralogical and geochemical composition of Arctic marine sediments is primarily controlled by the lithology of the surrounding continental source regions. As the principal sediment sources, these geologically diverse provinces bordering the Arctic Ocean impart distinct and diagnostic signatures to the adjacent marine environments (Stein, 2008; Harrison et al., 2008; Pease and Coakley, 2018; Myers and Darby, 2022).

The North American sector, encompassing the Canadian Arctic Archipelago and northern Alaska, is characterized by Precambrian rocks of the Canadian Shield, Paleozoic sedimentary successions of the Arctic Platform, and Mesozoic-Cenozoic orogenic belts associated with the North American Cordillera (Harrison et al., 2008). Geochemically, these ancient continental terrains are characterized by strongly negative εNd values and highly radiogenic $^{87}Sr/^{86}Sr$ ratios. They serve as the primary source of

Precambrian zircons and contribute substantial amounts of detrital carbonate minerals (e.g., dolomite and calcite) to the Arctic Ocean.

In contrast, the Eurasian sector exhibits a markedly different geological framework. The large drainage basins of major Siberian rivers, including the Ob, Yenisei, Lena and Kolyma rivers, erode the Mesozoic-Cenozoic sedimentary sequences of the Verkhoyansk-Chukotka region and extensive volcanic provinces, such as the Okhotsk-Chukotka Volcanic Belt (OCVB), the Kolyma-Omolon Belt and the Siberian Traps (Toro et al., 2016). As a result, sediments originating from these regions commonly yield more radiogenic εNd values, less radiogenic $^{87}Sr/^{86}Sr$ ratios, and abundant Mesozoic–Cenozoic zircon populations. Mineralogically, the Eurasian sector represents a major source of characteristic clay minerals, including illite derived from sedimentary rocks and smectite produced by the weathering of basalts, as well as distinctive detrital minerals (Stein, 2008). Furthermore, the Siberian and Baltic Cratons contribute materials derived from high-grade metamorphic rocks to the Laptev, Kara and Barents Seas. This pronounced lithological heterogeneity establishes unique sediment-source fingerprints for each marginal seas.

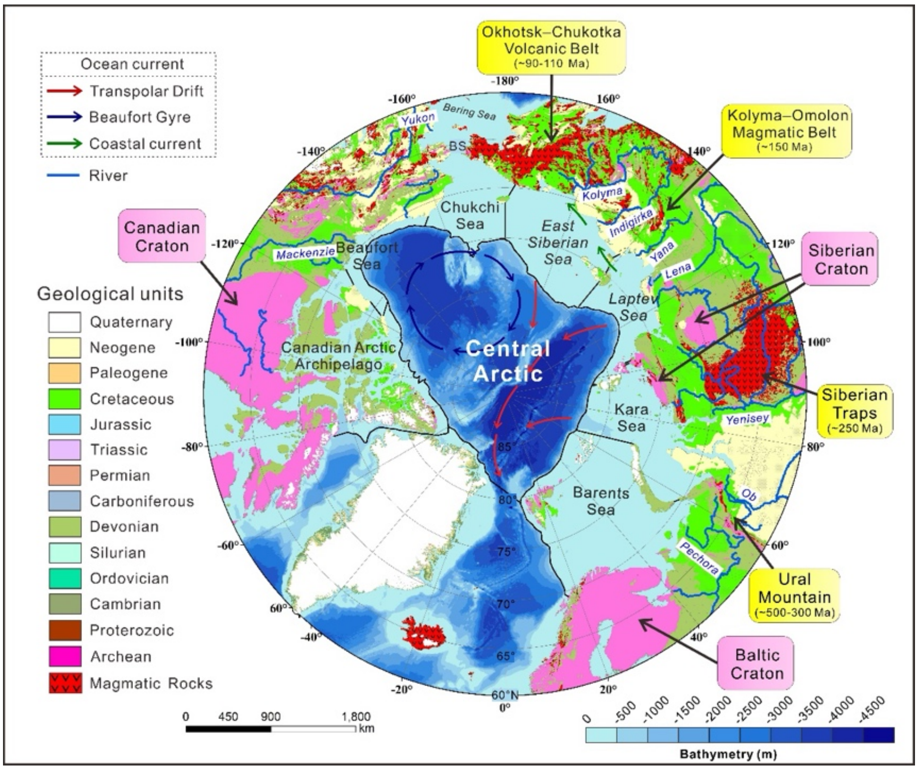

Figure 1. Overview map of the Arctic Ocean illustrating regional subdivisions and circum-Arctic lithological frameworks. The study area is divided into the central Arctic

Ocean and the Arctic marginal seas. The geological background is adapted from Harrison et al. (2011). Major magmatic and volcanic belts and cratons (Akinin et al., 2020) are indicated by arrows and annotated with colored boxes. BS denotes the Bering Strait. Major surface ocean circulation pathways are denoted by colored arrows, where red arrows indicate the Transpolar Drift, dark blue arrows indicate the Beaufort Gyre, and green arrows denote regional coastal currents (Timmermans and Marshall, 2020).

2.3 Dataset description

Surface sediment samples included in the CASPROD database were primarily collected from the uppermost layers (typically 0-2 cm to 0-5 cm). For sediment cores, the core-top intervals were used to represent the modern sedimentary conditions. All datasets are provided in standardized data table (Table 2) with a uniform metadata structure containing the following categories and fields. Station metadata: station identifier ("STATION"), geographical coordinates ("LAT" and "LON"), geographic region ("REGION"), sample position within the core or sediment column ("SAMPLE_PS"). Bathymetric information: water depth derived from shipboard measurement ("WATER_DEPTH") and from the GEBCO bathymetry ("GEBCO_DEPTH"). Water depth values were preferentially obtained from the original publications or cruise reports. For stations where shipboard depth information was unavailable, water depth was estimated using the GEBCO bathymetric grid. Provenance metadata: sample pretreatment methods ("PRETREATMENT"), analytical instrumentation ("INSTRUMENT"), and data source ("REFERENCE").

Although the depositional ages of these surface and core-top samples may vary slightly, they are all concentrated within the Holocene. Over this relatively short geological timescale, the primary circum-Arctic sediment source configurations and geological basements have remained remarkably stable. Consequently, any minor variation in depositional age among these surface and core-top sediments is practically negligible when utilizing CASPROD as a baseline to track provenance shifts over longer geological timescales, such as Quaternary glacial-interglacial cycles.

Table 1. CASPROD data from the central Arctic Ocean and marginal seas

Region*	Area* $10^3 km^2$	Sr-Nd isotope	Detrital zircon U-Pb Age	Clay minerals	Detrital minerals (XRD)	Detrital minerals (Counting)
1. Barents Sea	1626	12	1 (185)**	458	78	505
2. Kara Sea	942	15	5 (1263)	190	31	278
3. Laptev Sea	505	47	4 (846)	138	23	135
4. East Siberian Sea	1000	32	9 (1979)	113	27	533
5. Chukchi Sea	639	21	2 (398)	267	70	432
6. Beaufort Sea	183	4	1 (291)***	294	25	2
7. Canadian Arctic Archipelago	1171	9	0	6	55	0
8. Central Arctic Ocean	4500	35	0	181	168	103
Total（1-8）	10 566	175	21 (4671)	1647	477	1988

* Regional classification and corresponding area follow Martens et al. (2021). ** Numbers outside the parentheses indicate the number of samples, while numbers inside the parentheses denote the number of detrital zircon grains. *** The detrital zircon U-Pb age data for the Beaufort Sea were not obtained from the original source (Rino et al., 2004) and thus were not included in the total age statistics.

Table 2. Description of parameters and corresponding column headers in the CASPROD dataset

Parameters	Description	Column name
Sampling and Georeference information		
CASPROD entry ID	Serial number	ID
Station identifier	Expedition station ID	STATION
Latitude	Decimal latitude (WGS1984)	LAT
Longitude	Decimal longitude (WGS1984)	LON
Region	Central Arctic Ocean or marginal seas	REGION
Water depth (m.b.s.l.)	Water depth from shipboard measurement	WATER_DEPTH
Water depth based on GEBCO (m.b.s.l.)	Water depth according to GEBCO	GEBCO_DEPTH

Sample position (cm)	Sample depth below sediment-water interface	SAMPLE_PS
Sample Pretreatment	Chemical pre-treatment method	PRETREATMENT
Analytical Instrument	Instrument used for analysis	INSTRUMENT
Reference	Original publication of the data	REFERENCE
Sr-Nd isotopic data		
$^{87}Sr/^{86}Sr$	Measured $^{87}Sr/^{86}Sr$ ratio	SR
$^{144}Nd/^{143}Nd$	Measured $^{144}Nd/^{143}Nd$ ratio	ND
2σ	Two standard deviations	2S
εNd	$\varepsilon Nd = (^{143}Nd/^{144}Nd - 0.512638) / 0.512638 \times 10000$ (Jacobsen and Wasserburg, 1980)	εND
Zircon U-Pb data		
Zircon number	Number of zircon grains dated per sample	Z_NUM
90-110 Ma proportion	Proportion of 90-110 Ma zircon grains	90_110MA
140-160 Ma proportion	Proportion of 140-160 Ma zircon grains	140_160MA
220-360 Ma proportion	Proportion of 220-360 Ma zircon grains	220_360MA
420-560 Ma proportion	Proportion of 420-560 Ma zircon grains	420_560MA
1000-1500 Ma proportion	Proportion of 1000-1500 Ma zircon grains	1000_1500MA
1750-2000 Ma proportion	Proportion of 1750-2000 Ma zircon grains	1750_2000MA
Clay mineral data		
Smectite (%)	Smectite content	SME
Illite (%)	Illite content	ILL
Kaolinite (%)	Kaolinite content	KAO
Chlorite (%)	Chlorite content	CHL
Sample grain size	Particle size range used for testing	GS
Diffractometer	Diffractometer for testing	DFM
Slit	Slit used during testing	SLIT
Calculation software	Software for calculating mineral content	SOFTWARE
Comments	Necessary supplements	COMMENTS
Detrital mineral data		
Quartz (%)	Quartz content	QZ
Plagioclase feldspar (%)	Plagioclase feldspar content	PI
Potassium feldspar (%)	Potassium feldspar content	KFS
Calcite (%)	Calcite content	CAL
Dolomite (%)	Dolomite content	DOL
Siderite (%)	Siderite content	SD
Muscovite (%)	Muscovite content	MU

Biotite (%)	Biotite content	BI
Glauconite (%)	Glauconite content	Glt
Pyroxene (%)	Pyroxene content	PX
Amphibole (%)	Amphibole content	AM
Garnet (%)	Garnet content	GRT
Staurolite (%)	Staurolite content	ST
Andalusite (%)	Andalusite content	AND
Kyanite (%)	Kyanite content	KY
Sillimanite (%)	Sillimanite content	SIL
Epidote (%)	Epidote content	EP
Chloritoid (%)	Chloritoid content	CLD
Prehnite (%)	Prehnite content	PRH
Zeolite (%)	Zeolite content	ZEO
Serpentine (%)	Serpentine content	SRP
Actinolite (%)	Actinolite content	ACT
Zircon (%)	Zircon content	ZRN
Tourmaline (%)	Tourmaline content	TUR
Rutile (%)	Rutile content	RT
Titanite (%)	Titanite content	TTN
Apatite (%)	Apatite content	AP
Anatase (%)	Anatase content	ANT
Magnetite (%)	Magnetite content	MAG
Hematite (%)	Hematite content	HEM
Limonite (%)	Limonite content	LIM
Ilmenite (%)	Ilmenite content	ILM
Pyrite (%)	Pyrite content	PY
Barite (%)	Barite content	BRT
Spinel (%)	Spinel content	SPL

2.4 Dataset parameters

The CASPROD database integrates four primary provenance proxy categories, providing key multi-proxy data to constrain sediment sources and transport pathways within the Arctic Ocean: Sr–Nd isotopes, detrital zircon U–Pb ages, clay mineral assemblages, and detrital mineral compositions (Table 2). The clay mineralogy dataset reports the relative abundances of four major groups: kaolinite, illite, smectite, and chlorite. The detrital mineral dataset comprises a diverse suite of mineral types, generally categorized into heavy- and light-mineral fractions (Table 2). All compiled datasets are publicly accessible through the repository described in the Data Availability section.

2.5 Data sources and quality assurance

The CASPROD dataset synthesizes data from 117 previously published studies and publicly available databases, all of which are fully and appropriately cited. To ensure complete traceability, each data record is explicitly linked to its original source reference within the primary data tables. A comprehensive bibliography of all source publications is provided in the Supplement. Furthermore, to enable rigorous user-assessed quality, the database documents detailed metadata for each record. For detrital zircon and detrital mineral data obtained through microscopic identification, the corresponding pre-treatment methods and instruments are provided. For clay mineral and detrital data derived from XRD analysis, the dataset includes pre-treatment procedures, XRD instruments (including the type of X-ray tube, e.g., Cu or Co), whether the slit system is automatic or fixed, and the software used for data calculation.

2.6 Data interpolation

To facilitate spatial analysis and visualization, the CASPROD database provides interpolated raster products (GeoTIFF format) for Sr-Nd isotopes, clay mineral assemblages, and detrital mineral distributions. All spatial data are projected using the WGS 1984 Arctic Polar Orthographic projection to minimized distortion at high latitudes. Interpolation was performed using Ocean Data View software (ODV; Schlitzer, 2022), specifically employing the Data-Interpolating Variational Analysis (DIVA) method (Brasseur et al., 1996; Troupin et al., 2012). DIVA is a variational interpolation technique that estimates continuous fields by optimizing a cost function to balances data fidelity, field smoothness, and consistency with physical boundaries constraints such as complex coastlines. In contrast to traditional kriging methods, DIVA explicitly accounts for anisotropic spatial correlations and incorporates boundary conditions, making it exceptionally suitable for oceanographic datasets characterized by complex basin geometries and irregular data coverage. As implemented in ODV, DIVA allows user-defined correlation lengths in both longitudinal and latitudinal directions, generates gridded estimation error fields, and supports isopycnic gridding when density-based coordinates are applied. Consequently, this approach improves the representation of spatial gradients in regions with heterogeneous data coverage, particularly between the Arctic shelf seas and central deep basins.

Although the DIVA method successfully integrates topographic features and complex coastlines to optimize spatial continuity, the accuracy of the interpolated values remains highly dependent on data density. In well-sampled regions, such as the Chukchi Sea, Laptev Sea, and parts of the Barents-Kara Seas, the grid cells represent robust local signals. Conversely, in regions with sparse sampling coverage, most notably parts of the deep Canada Basin and portions of the Canadian Arctic Archipelago, the interpolated values carry relatively higher uncertainty. Consequently, the interpolated results in these data-sparse or unsampled areas should be treated with caution and utilized primarily as a qualitative reference.

3. Results and discussion

3.1 Dataset inventory and spatial distribution

This section presents an overview of the CASPROD database inventory and examines the spatial distribution of the four primary provenance proxy groups across the Arctic Ocean. By systematically mapping the data coverage across the Arctic Ocean, we highlight regional variations in data density and identify areas where information remains limited. The geographical patterns of key geochemical and mineralogical parameters are illustrated using a series of maps and diagrams.

3.1.1 Sr-Nd Isotopes

The Sr-Nd isotopic dataset comprises 175 data points from detrital component of surface sediments, with εNd values ranging from -19.5 to -4.0 and $^{87}Sr/^{86}Sr$ ratios from 0.710 to 0.745. A composite map that overlays all sample locations with the interpolated spatial distributions of $^{87}Sr/^{86}Sr$ ratio and εNd values, revealing a pronounced contrast between the two major Arctic sectors (Figure 2). The North American sector exhibits higher $^{87}Sr/^{86}Sr$ ratios and lower εNd values relative to the Eurasian sector. Specifically, the North American margin features evolved crustal signals, with mean values observed in the Canadian Arctic Archipelago (εNd = -14.7, $^{87}Sr/^{86}Sr$ = 0.728), and Beaufort Sea (εNd= -14.4, $^{87}Sr/^{86}Sr$ = 0.731). In contrast, sediments from the Eurasian marginal seas exhibit systematically higher εNd values and lower $^{87}Sr/^{86}Sr$ ratios. Representative mean values include the Barents Sea (εNd = -10.7, $^{87}Sr/^{86}Sr$ = 0.722), Kara Sea (εNd = -7.9, $^{87}Sr/^{86}Sr$ = 0.717), Laptev Sea (εNd = -12.0, $^{87}Sr/^{86}Sr$ = 0.716), East Siberian Sea (εNd = -9.5, $^{87}Sr/^{86}Sr$ = 0.714), and Chukchi Sea (εNd = -8.0, $^{87}Sr/^{86}Sr$ = 0.712).

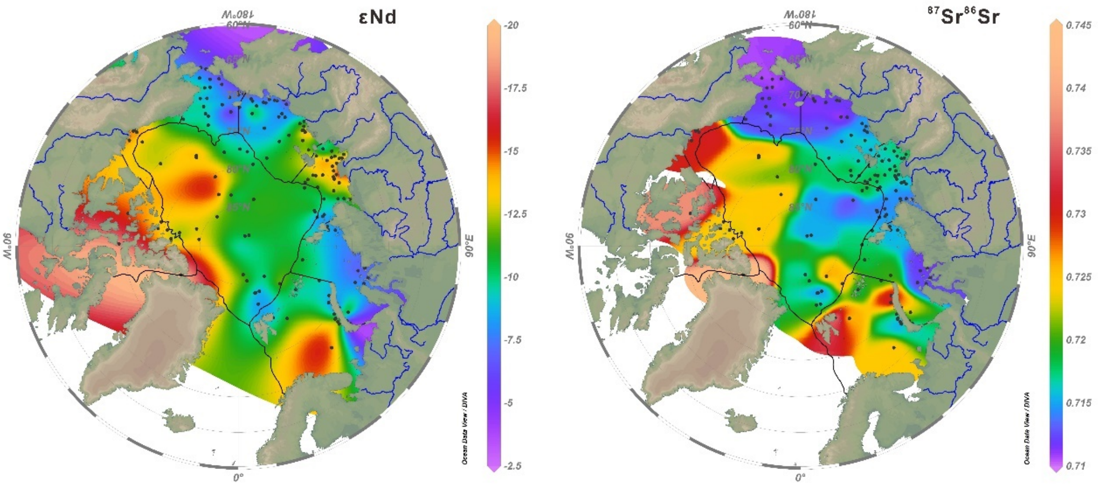

Figure 2. Spatial distribution of εNd and $^{87}Sr/^{86}Sr$ in surface sediments of the Arctic Ocean. Note that some marginal parts of the distribution maps do not contain data points but are the result of extrapolation by the Ocean Data View software.

3.1.2 Zircon U-Pb Ages

The detrital zircon U-Pb ages dataset comprises 22 surface sediment samples, yielding 4671 ages. Age distributions for each marginal seas are visualized using frequency histograms and kernel density estimation (KDE) plots (Figure 3). While original zircon age data for the Beaufort Sea are unavailable, the zircon age distribution was derived by digitizing the figure from Rino et al. (2004). These distribution patterns reveal distinct regional provenance signatures across the circum-Arctic marginal seas. A common Paleoproterozoic age peak at ~1750–2000 Ma is evident throughout the Arctic basin, whereas the North American sector is uniquely characterized by a Mesoproterozoic population (1000–1500 Ma) that is absent in Eurasian margin sediments. In contrast, sediments from the Eurasian marginal seas display distinctive younger zircon age populations. The Barents and Kara Seas are characterized by prominent peaks at 220–360 Ma and 420–560 Ma, whereas the Laptev Sea shows dominant populations at 140–160 Ma and 220–360 Ma. Even younger detrital zircon signatures are evident in the East Siberian and Chukchi Seas, where age spectra are dominated by a pronounced peak at 90–110 Ma.

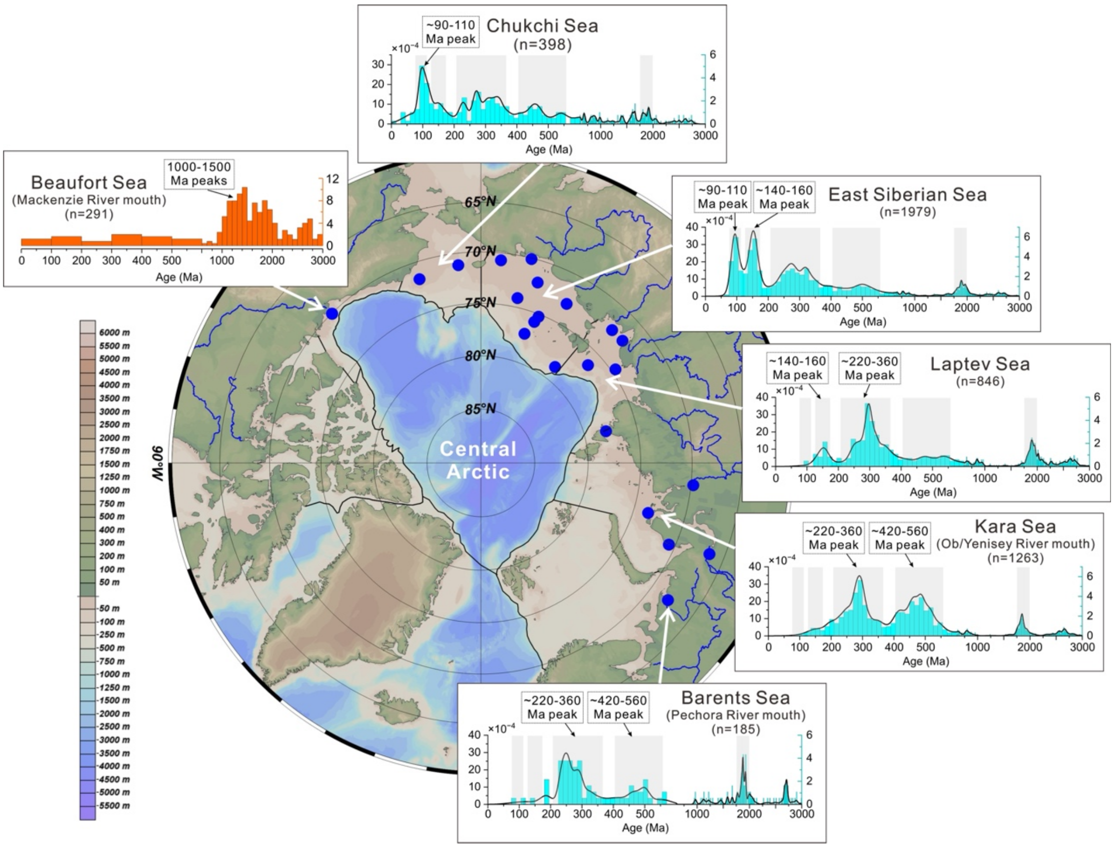

Figure 3. Station map and detrital zircon U-Pb age distribution in surface sediments of the Arctic Ocean

3.1.3 Clay Mineral Assemblages

The clay mineralogy dataset (n=1647) records the relative abundances (%) of four principal mineral groups: illite, smectite, kaolinite, and chlorite. Spatially interpolated maps for each mineral (Figure 4) reveal distinct basin-scale fractionation patterns. Smectite concentrations are notably higher in the Kara Sea (mean 38.9%), with secondary peaks in the Canadian Arctic Archipelago (17.2%), and the Laptev Sea (17.7%). Kaolinite is elevated primarily in the Barents Sea (14.0%) and the Beaufort Sea (10.6%), while illite dominates the eastern Arctic, particularly in the East Siberian (66.3%), Beaufort (60.6%) Seas and Chukchi (53.8%). Unlike the other minerals, chlorite displays a relatively uniform distribution throughout the Arctic marginal seas, with average values ranging narrowly from 17.3% to 23.3%. These mean values for the circum-Arctic marginal seas are quite similar to those listed in Stein (2008).

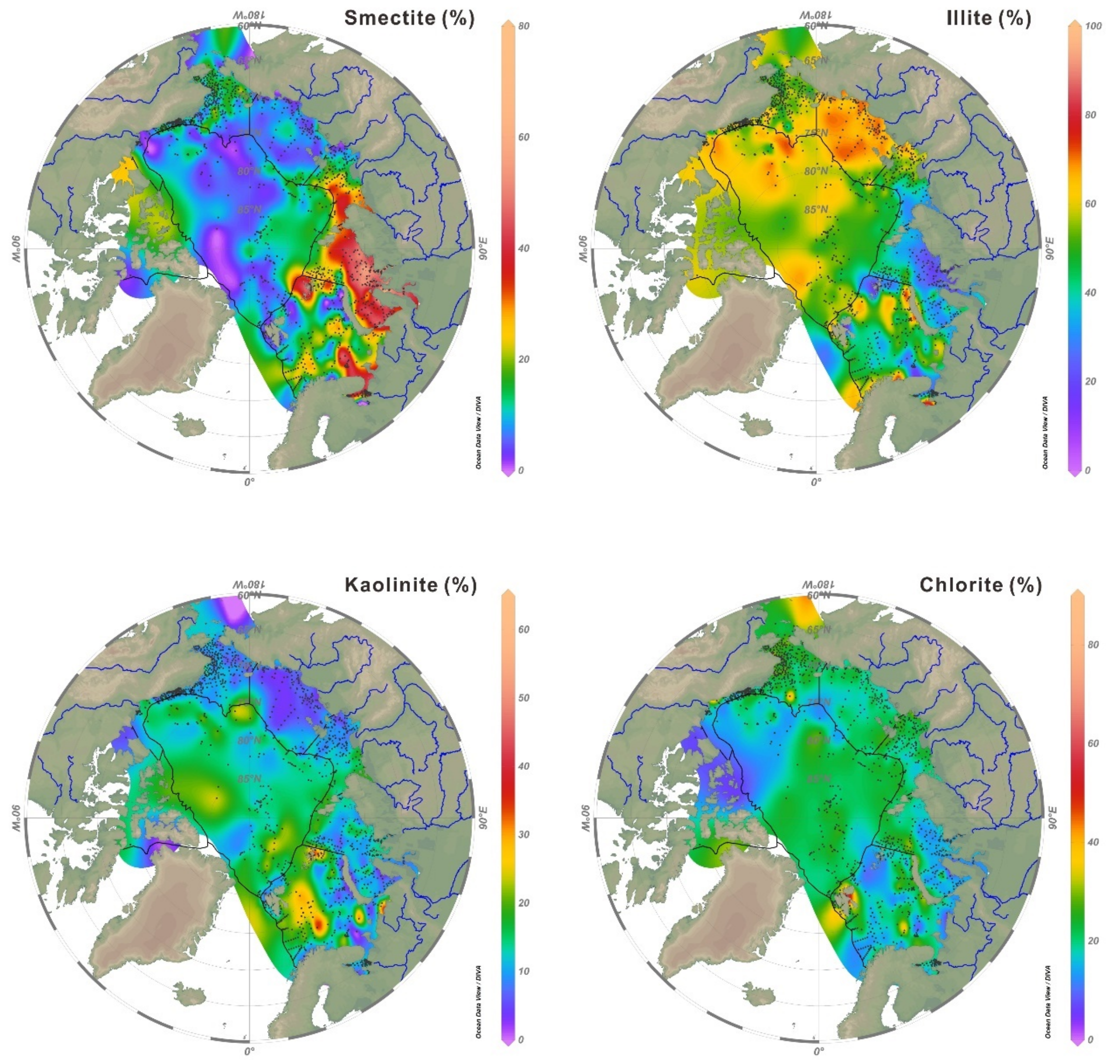

Figure 4. Spatial distribution of major clay minerals (Smectite, Illite, Kaolinite, and Chlorite) in surface sediments of the Arctic Ocean. Note that some marginal parts of the distribution maps do not contain data points but are the result of extrapolation by the Ocean Data View software.

3.1.4 Detrital Mineral Assemblages

The detrital mineral dataset contains 2465 analyses that characterize both light (e.g., quartz, feldspar, dolomite) and heavy mineral fractions (e.g., amphibole, pyroxene, garnet, staurolite). These data were obtained using from two complementary analytical approaches: X-ray diffraction (XRD, n=477) and optical counting (n=1988). Figure 5 presents distribution maps of key provenance-sensitive minerals, illustrating significant regional heterogeneity across the Arctic margins. Among the light minerals fraction, quartz is most abundant in the Beaufort (35.9%), Kara (34.2%), and Laptev (33.8%)

Seas. Plagioclase enrichment is characteristic of the Laptev (25.8%), Kara (22.9%), and East Siberian (19.5%) Seas, whereas potassium feldspar (K-feldspar) concentrations are elevated in the Canadian Arctic Archipelago (10.0%), the Laptev Sea (8.9%), and the Kara Sea (6.7%). Notably, carbonate signals, specifically dolomite, are distinctly enriched in the North American sector, the Canadian Arctic Archipelago (11.0%) and the Beaufort Sea (5.5%).

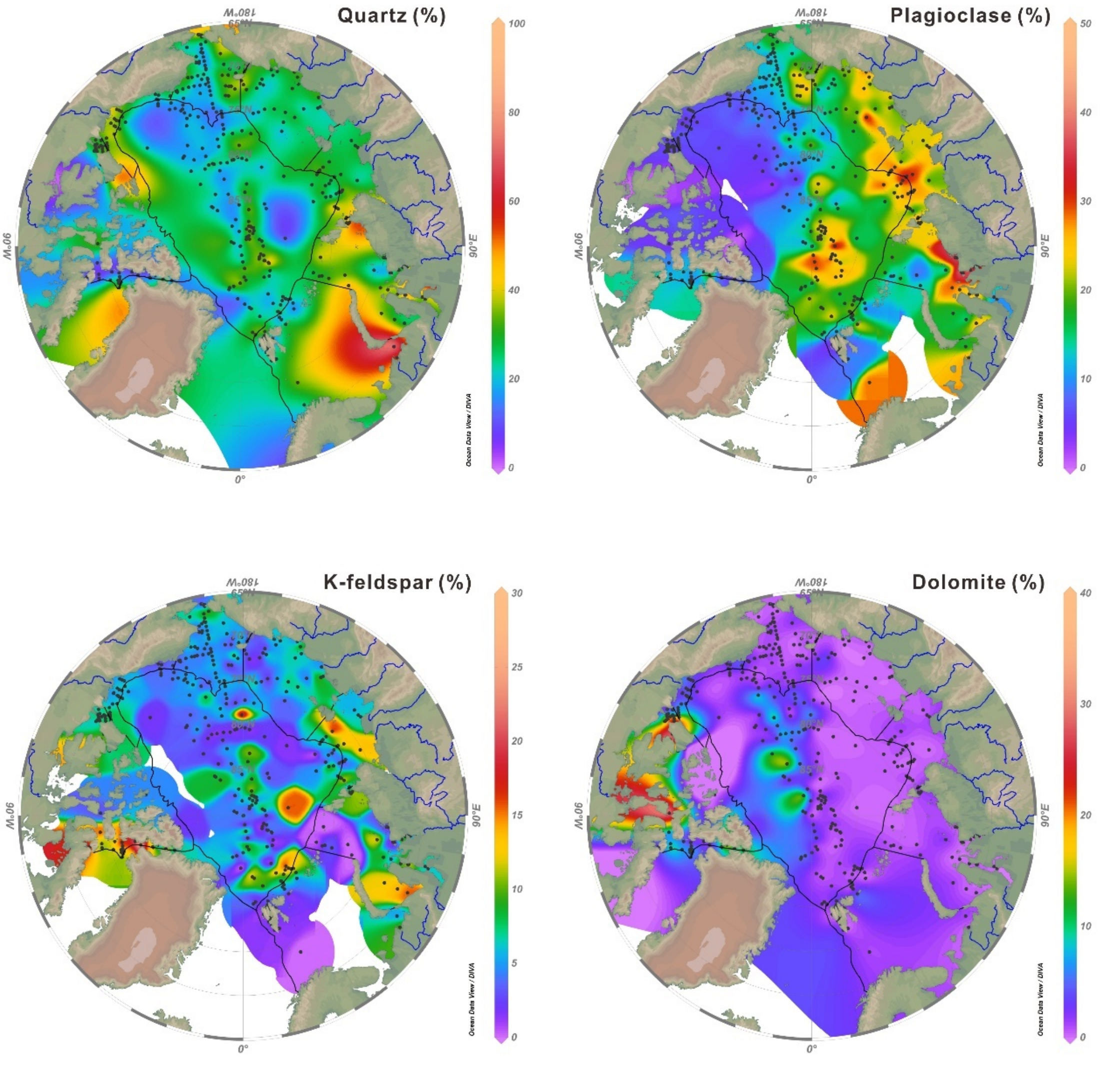

Figure 5. Spatial distribution of key light minerals (Quartz, Plagioclase, K-feldspar, and Dolomite) in surface sediments of the Arctic Ocean. Note that some marginal parts of the distribution maps do not contain data points but are the result of extrapolation by the Ocean Data View software.

Within the heavy mineral fraction, pyroxene concentrations peak in the eastern

Arctic, notably the Kara (20.5%) and Laptev Seas (20.2%), as well as in areas adjacent to Franz Josef Island near the Kara-Barents sector. Amphibole dominates the heavy mineral fraction in the Laptev Sea (27.4%), followed by the East Siberian Sea (17.7%), and the Chukchi Sea (14.8%), and is also rich in southern Barents Sea. Metamorphic indicators, such as garnet, are elevated in the Barents (8.9%), Laptev (7.1%), and Kara (5.6%) Seas, while epidote shows relative enrichment in the Chukchi (19.7%) and Barents Seas (11.9%).

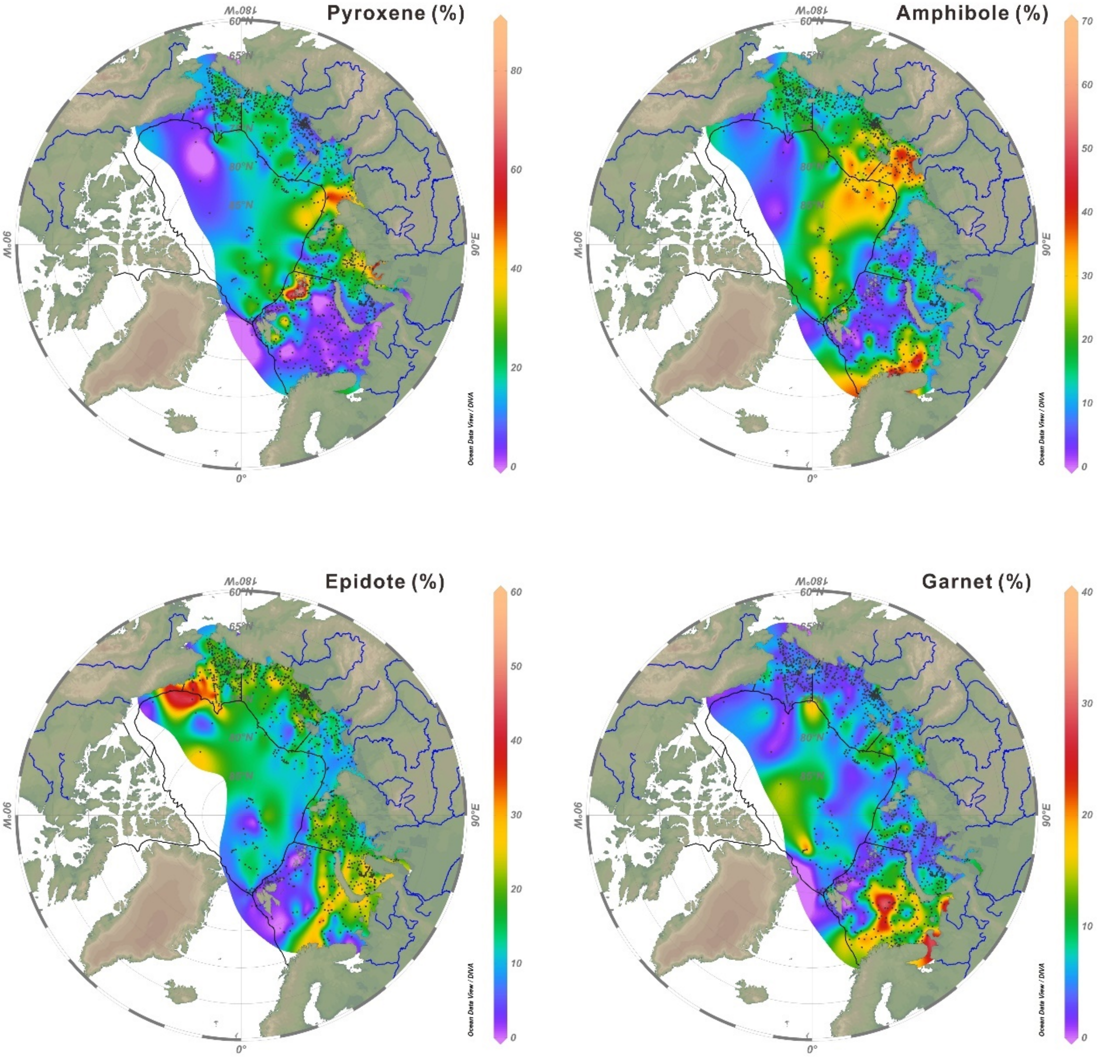

Figure 6. Spatial distribution of key heavy minerals (Pyroxene, Amphibole, Epidote, and Garnet) in surface sediments of the Arctic Ocean. Note that some marginal parts of the distribution maps do not contain data points but are the result of extrapolation by the Ocean Data View software.

3.2 *Circum-Arctic provenance implications*

The multi-proxy synthesis in CASPROD effectively links shelf deposits with the geological characteristics of their respective hinterlands, providing critical fingerprints to trace pan-Arctic sediment transport. The Sr-Nd isotopic compositions reflect the crustal residence age of source rocks (White, 2013). High $^{87}Sr/^{86}Sr$ ratios and low εNd values in the Canadian Arctic Archipelago, Beaufort, Barents, and Laptev Seas define a characteristic "cratonic" signature, indicative of sediment contributions from ancient Archean basement rocks, including North America, Baltica, and Siberia (Bazhenova et al., 2017). Conversely, the Eurasian sector exhibits "younger" isotopic signatures. The unradiogenic $^{87}Sr/^{86}Sr$ and relatively high εNd values in the Kara, East Siberian and Chukchi Seas successfully trace sediment inputs derived from the Permian-Triassic Siberian Large Igneous Province (SLIP; Tütken et al., 2002) and the Jurassic-Cretaceous OCVB (Li et al., 2023).

Zircon U-Pb age spectra provide further constrain on sediment provenance by identifying the formation ages of felsic igneous rocks in the source regions (Moecher and Samson, 2006). The North American sector, particularly areas influenced by the Mackenzie River system, is uniquely distinguished by a prominent 1000–1500 Ma age population, diagnostic of the Grenville Orogeny (Rino et al., 2004). In contrast, zircon age distributions across the Eurasian sector are dominated by Phanerozoic populations, that trace distinct regional geological events. These include prominent Paleozoic peaks (220–360 Ma and 420–560 Ma) in the Barents and Kara Seas associated with the erosion of the Ural Mountains and Central Asian Orogenic Belt (Puchkov and Ivanov, 2020; Parfenov et al., 2009; Campbell et al., 1992), and Mesozoic peaks (90–160 Ma) in the East Siberian and Chukchi Seas that trace magmatic activity associated with the OCVB (Akinin et al., 2020).

Clay and detrital mineral assemblages provide complementary insights into circum-Arctic lithologies and physical weathering domains. Smectite is enriched in the Kara and Laptev Seas, reflecting the erosion of basalts from the SLIP basalts (e.g., Rossak et al., 1999; Wahsner et al., 1999; Stein et al., 2004), while its elevated abundances in the Canadian Arctic Archipelago indicate local erosion of exposed mafic gabbros (Kingsbury et al., 2018). Kaolinite signals the reworking of ancient weathering crusts, with major sources tied to Triassic-Jurassic sedimentary rocks on Franz Josef Land (Elverhøi et al., 1989; Vogt and Knies, 2009) and the weathered North American Craton supplying the Canadian Arctic Archipelago (Stevenard et al., 2022). Hight illite contents in the East Siberian, Chukchi, and Beaufort Seas delineate dominant physical weathering of mixed sedimentary, metamorphic, and felsic igneous lithologies (e.g., Viscosi-Shirley et al., 2003a; Stein, 2008).

Light and heavy mineral fractions further refine the provenance interpretations. Plagioclase is particularly enriched in the Kara, Laptev, and East Siberian Seas, reflecting inputs from the SLIP and OCVB. Potassium feldspar indicates granitic or gneissic sources, linking sediments in the Laptev Sea and western Kara Seas to erosion of the Siberian Craton and Uralian basement, respectively (Vogt, 1997). Quartz dominates in regions with limited igneous influence, such as areas affected by the Pechora River and Mackenzie River system and the Taimyr-Severnaya Zemlya fold belt. Dolomite enrichment in the Canadian Arctic Archipelago provides a clear fingerprint of local Cambrian-Devonian carbonate bedrocks erosion (Clark et al., 1980; Vogt, 1997; Phillips and Grantz, 2001; Stein et al., 2010; Bazhenova et al., 2017).

Within the heavy mineral fraction, pyroxene serves as a diagnostic mafic tracer (Garzanti and Andò, 2007), linking sediments near Franz Josef Land to local mafic igneous outcrops and sediments in the Kara and Laptev Seas to erosion of the Siberian Traps (Behrends, 1999; Wang et al., 2022). High-grade metamorphic indicator minerals, such as garnet and amphibole (Behrends, 1999; Garzanti and Andò, 2007), are abundant in the Barents, Kara, and Laptev Seas, reflecting erosion of crystalline basement from the Baltic and Siberian Cratons, especially the Taimyr region.

Stein (2008) documented the spatial distribution patterns of four clay minerals (illite, smectite, chlorite, and kaolinite) and four detrital minerals (amphibole, clinopyroxene, epidote, and garnet) across the Arctic Ocean (for database and down-load see Stein, 2026a, 2026b). Furthermore, lower-resolution distribution maps of the detrital minerals quartz, plagioclase, kalifeldspar and dolomite of surface sediments from the central Arctic Ocean and the Laptev and Kara seas are also presented in Stein (2008), based on data from Vogt (1997). Compared with the database compiled by Stein (2008), the overall spatial distribution patterns as well as mean concentrations of both clay and detrital minerals in our new dataset remain largely consistent, confirming the robustness of the earlier synthesis of mineralogy. However, the present compilation incorporates recently published data from the Canada Basin (e.g., Deschamps et al., 2018), the Canadian Arctic Archipelago (e.g., Myers and Darby, 2022), the Chukchi Sea (e.g., Li et al., 2021), the East Siberian Sea (e.g., Wang et al., 2024), and the Barents Sea (e.g., Vogt and Knies, 2009), thereby improving spatial coverage across key Arctic marginal seas. The inclusion of these new datasets enables a higher-resolution and more refined characterization of mineral distribution patterns in regions that were less well constrained in Stein (2008), particularly over the East Siberian Sea shelf and within the Canada Basin. In addition, we expand the analysis to include a broader suite of provenance-sensitive detrital minerals, such as quartz, plagioclase, K-feldspar, dolomite, pyroxene, and staurolite, further strengthening source-to-sink interpretations.

3.3 Evaluating the discriminability of provenance proxies

Provenance accuracy is method-dependent and is linked to the analytical unit of a given proxy. For single-grain techniques like Fe-oxide chemical fingerprinting, accuracy is typically evaluated through cross-validation against a reference to quantify incorrect source assignments (Darby et al., 2015). However, this traditional concept of accuracy is not directly applicable to the integrated-signal proxies compiled in CASPROD (e.g., Sr-Nd isotopes, clay and detrital minerals, and zircon U-Pb ages), which yield bulk or distributional signatures of sediment mixtures rather than discrete grain labels. Instead, we evaluate these proxies based on discriminability, defined here as the signal-to-noise ratio (SNR) between inter-source differences and intra-source variability (Figure 7). A high SNR (generally >1) indicates that the compositional contrast between two sources substantially outweighs their internal natural heterogeneity, allowing for reliable provenance discrimination, with larger values yielding greater discriminability.

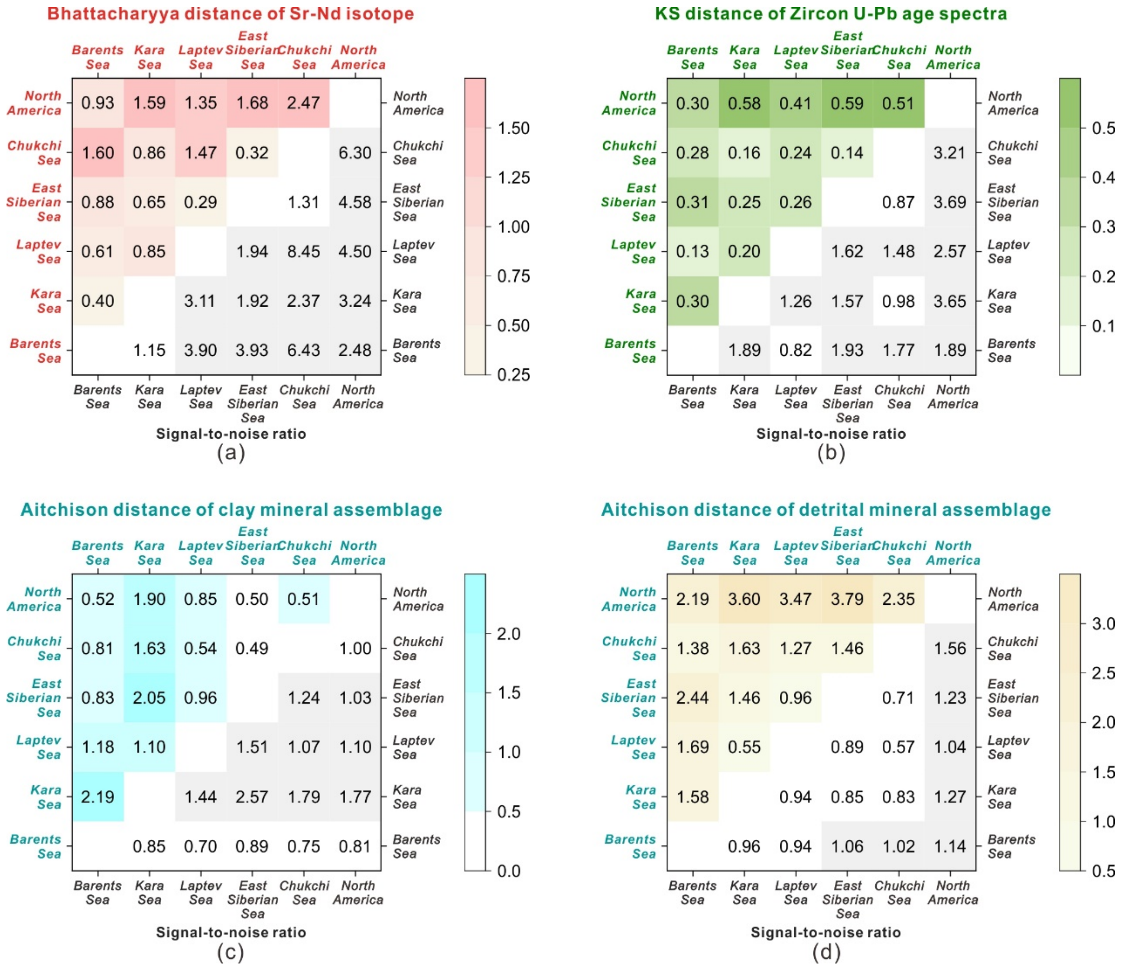

Figure 7. Distance matrix heatmaps illustrating the discriminability of four provenance proxies. In each panel, the upper and lower triangle display pairwise inter-source distances and the corresponding signal-to-noise ratios (SNR), respectively. SNR is defined as the ratio of inter-source distance to intra-source variability. Gray shaded cells denote high SNR values (>1), indicating that the corresponding two source regions can be effectively differentiated by the given proxy. KS: Kolmogorov–Smirnov.

To evaluate pairwise source-region distances and intra-source heterogeneity, we selected statistical metrics tailored to the specific data structure of each proxy. For Sr-Nd isotopes, we applied the Bhattacharyya distance (Bhattacharyya, 1946) to measure source separation in the bivariate εNd–$^{87}Sr/^{86}Sr$ space, as it accommodates substantial differences in data dispersion among source areas without assuming identical covariance structures. For detrital zircon U-Pb age spectra, we used the Kolmogorov–

Smirnov (KS) distance. As a distribution-free metric quantifying the maximum vertical difference between two cumulative age-distribution functions, the KS distance is highly sensitive to overall spectral shape and serves as a standard for nonparametric age-spectrum comparisons (Vermeesch, 2012). For clay mineral and detrital mineral assemblages, we applied the Aitchison distance to measure compositional differences between source regions, because percentage of minerals are subject to the constant-sum constraint and conventional distance metrics would introduce spurious correlations (Garzanti et al., 2012). Across all proxies, intra-source heterogeneity is represented by the median distance derived from 1000 bootstrap resampling iterations within each source group.

The calculated SNR values reveals that low discriminability typically stems from substantial signal overlap between specific regions (Figure 7). For instance, detrital zircon U-Pb age spectra cannot effectively differentiate the Kara, Chukchi, and East Siberian seas, nor can they separate the Barents Sea and Laptev Sea (Fig. 7b). This overlap occurs because these marginal seas collectively drain extensive Phanerozoic magmatic provinces, such as the Siberian Traps and the Okhotsk–Chukotka Volcanic Belt, yielding highly convergent age distributions. Similarly, clay mineral assemblages show limited discriminability for the Barents Sea (Figure. 7c), reflecting pronounced intra-regional spatial variability driven by complex hydrodynamics and the mixing of diverse local endmembers. Detrital mineral assemblages also struggle to distinguish Eurasian interior sources, particularly the Kara, Laptev, and East Siberian seas (Figure. 7d). Sr-Nd isotopes, despite generally exhibiting high SNR values (>1), show limited discriminability between the East Siberian and Chukchi seas, or the Barents and Kara seas (Figure. 7a), underscoring the challenge of differentiating provenance with similar geological affinities.

These overlaps highlight the inherent limitations of relying on any single proxy to decipher a complex, multi-source sedimentary system like the Arctic Ocean. Accurate circum-Arctic provenance reconstruction requires a multi-proxy approach (e.g., Stein, 2008; Myers and Darby, 2022). Thus, in several studies multi-proxy approaches have been used to identify circum-Arctic sediment provenances more accurately, e.g. the combination of heavy minerals, clay minerals and major and minor elements (Schoster et al., 2000; Viscosi-Shirley et al., 2003a, 2003b) or the combination of heavy minerals, clay minerals, and chemical fingerprinting of major and minor elements in Fe-oxide minerals (Myers and Darby, 2022).

CASPROD also establishes a multi-proxy, cross-validation framework to overcome the ambiguity introduced by these overlapping signatures. By synthesizing geochemical, geochronological, and mineralogical datasets, this integrated framework provides multiple constraints on endmembers and substantially improve the accuracy of provenance identification. Furthermore, to achieve higher accuracy when interpretating highly complex mixed signals, particularly regarding ice-rafted debris, we encourage database users to couple CASPROD with other approaches, such as the Fe-oxide grain chemical fingerprinting method (Darby, 2003; Darby et al.; 2015; Myers and Darby, 2022).

4. Data availability

The CASPROD dataset is publicly available at Figshare (https://doi.org/10.6084/m9.figshare.31926927; Yao et al., 2026) and is provided under an open-access license. All relevant contact information and metadata documentation are provided on the website. The scientific community is encouraged to contribute new and updated datasets to CASPROD, enabling continuous expansion and updates of this resource.

5. Conclusions and outlook

The CASPROD database is one of the most comprehensive compilations of sensitive provenance-related data for Arctic surface sediments currently available. By integrating mineralogical parameters with key geochemical tracers, such as Sr-Nd isotopes and detrital zircon U-Pb ages, CASPROD establishes a valuable framework for characterizing sediment sources across the circum-Arctic margins. While individual provenance proxies reflect specific aspects of source lithology and weathering regimes, these signals are inherently modified by sediment mixing, transport processes (riverine input, sea-ice rafting and ocean circulation), and hydrodynamic sorting within the

Arctic Ocean. As a result, interpretations based on a single proxy can be ambiguous, particularly in regions where source signatures overlap. A multi-proxy strategy such as implemented in CASPROD is therefore essential. Integrating complementary tracers-especially also in combination with other sediment provenance indicators such as Fe-oxide fingerprinting and multi-element chemistry - improves the discrimination of potential sources and enables quantitative unmixing, provided end-member compositions are well-constrained. Ultimately, this integrated framework not only elucidates modern sediment source-to-sink process but also provides a critical baseline for reconstructing Quaternary environmental changes, including ice-sheet dynamics, sea-ice variability, and ocean circulation. As such, CASPROD constitutes a valuable and enduring resource for advancing research in Arctic marine geology, paleoclimatology, and Earth system science.

Supplement. The supplementary materials related to this article is available online.

Author Contributions. ZY conceived and designed the study. ZY and HF were responsible for the construction of the database. RS, YL, XS, YV, SN, LD, FS, KW, ZC, SQ, QL, SZ, XP, HG, YL contributed to data collection, database construction, and verification. ZY drafted the manuscript. All authors contributed to the writing and editing of the manuscript.

Competing interests. The authors declare that they have no conflict of interest.

Acknowledgements. We thank the crew members and scientific participants of the Chinese-Russian joint expedition cruises and the Chinese Arctic Research Expeditions for their efforts in sample collection. We are also grateful to the scientists who contributed data to the CASPROD database. We are particularly indebted to Christoph Vogt for his guidance in compiling the clay mineral dataset. This work was supported by the National Natural Science Foundation of China (42525606), the National Key Research and Development Program of China (2023YFF0804600), the Basic Scientific Fund for National Public Research Institutes of China (2026S08), and the Russian state budget (124022100084-8 of the POI FEB RAS).

References

Akinin, V. V., Miller, E. L., Toro, J., Prokopiev, A. V., Gottlieb, E. S., Pearcey, S., Polzunenkov, G. O., and Trunilina, V. A.: Episodicity and the dance of late Mesozoic magmatism and deformation along the northern circum-Pacific margin: north-eastern Russia to the Cordillera, Earth Sci. Rev., 208, 103272, https://doi.org/10.1016/j.earscirev.2020.103272, 2020.

Andrews, J. T.: Baffin Bay/Nares Strait surface (seafloor) sediment mineralogy, Further investigations and methods to elucidate spatial variations in provenance, Can. J. Earth Sci., 56, 814-828, https://doi.org/10.1139/cjes-2018-0207, 2019.

Bazhenova, E. A.: Reconstruction of late Quaternary sedimentary environments at the southern Mendeleev Ridge (Arctic Ocean), Ph.D. thesis, Fakultät für Geowissenschaften, University of Bremen, Bremen, Germany, 83 pp., https://hdl.handle.net/10013/epic.dec92c3a-3ec6-4ead-87e1-bd77301c604c, 2012.

Bazhenova, E., Fagel, N., and Stein, R.: North American origin of “pink－white” layers at the Mendeleev Ridge (Arctic Ocean): New insights from lead and neodymium isotope composition of detrital sediment component, Mar. Geol., 386, 44-55, https://doi.org/10.1016/j.margeo.2017.01.010, 2017.

Behrends, M.: Reconstruction of sea-ice drift and terrigenous sediment supply in the Late Quaternary: Heavy-mineral associations in sediments of the Laptev-Sea continental margin and the central Arctic Ocean, Reps. Pol. Res., 310, 167 pp., https://epic.awi.de/id/eprint/26490/, 1999.

Bhattacharyya, A.: On a Measure of divergence between two multinomial populations. Sankhyā: Indian J. Stat., 7, 401-406, 1946.

Brasseur, P., Beckers, J.-M., Brankart, J.-M., and Schoenauen, R.: Seasonal temperature and salinity fields in the Mediterranean Sea: Climatological analyses of an historical data set, Deep-Sea Res. Pt. I, 43, 159–192, https://doi.org/10.1016/0967-0637(96)00012-X, 1996.

Campbell, I. H., Czamanske, G. K., Fedorenko, V. A., Hill, R. I., and Stepanov, V.: Synchronism of the Siberian Traps and the Permian-Triassic Boundary, Sci., 258, 1760-1763, https://doi.org/10.1126/science.258.5089.1760, 1992.

Clark, D. L., Whitman, R. R., Morgan, K. A., and Mackey, S. D.: Stratigraphy and glacial marine sediments of the Amerasian Basin, central Arctic Ocean, Geol. Soc. Am. Spec. Pap. 181, 57 pp., https://doi.org/10.1130/SPE181-p1, 1980.

Cofield, S. and Darby, D.: History of the Barents Sea Ice Sheet, MIS 11 to present, Quat. Sci. Rev., 370, 109684, https://doi.org/10.1016/j.quascirev.2025.109684, 2025.

Cohen, J., Screen, J. A., Furtado, J. C., Barlow, M., Whittleston, D., Coumou, D., Francis, J., Dethloff, K., Entekhabi, D., Overland, J., and Jones, J.: Recent Arctic amplification and extreme mid-latitude weather. Nat. Geosci., 7, 627-637, https://doi.org/10.1038/ngeo2234, 2014.

Darby, D.A. and Bischof, J.F.: A statistical approach to source determination of lithic and Fe oxide grains: An example from the Alpha Ridge, Arctic Ocean. J. Sed. Res., 66, 599-607, 1996.

Darby, D. A., Myers, W., Herman, S., and Nicholson, B.: Chemical fingerprinting, a precise and efficient method to determine sediment sources, J. Sediment. Res., 85, 247–253, https://doi.org/10.2110/jsr.2015.17, 2015.

Darby, D. A.: Ephemeral formation of perennial sea ice in the Arctic Ocean during the middle Eocene, Nat. Geosci., 7, 210–213, https://doi.org/10.1038/ngeo2090, 2014.

Darby, D. A.: Sources of sediment found in sea ice from the western Arctic Ocean: New insights into processes of entrainment and drift patterns, J. Geophys. Res. Oceans, 108, 3257, https://doi.org/10.1029/2002JC001350, 2003.

Deschamps, C., Montero-Serrano, J., and St-Onge, G.: Sediment Provenance Changes in the Western Arctic Ocean in Response to Ice Rafting, Sea Level, and Oceanic Circulation Variations Since the Last Deglaciation, Geochem. Geophy. Geosy., 19, 2147-2165, https://doi.org/10.1029/2017GC007411, 2018.

Dong L., Shi X., Liu Y., Fang X., Chen Z., Wang C., Zou J., Huang Y.: Minerals in surface sediments in the western Arctic Ocean and their sources (in Chinese), Chin. J. Polar Res., 26, 58-70, https://doi.org/10.13679/j.jdyj.2014.1.058, 2014.

Eicken, H., Gradinger, R., Gaylord, A., Mahoney, A., Rigor, I., and Melling, H.: Sediment transport by sea ice in the Chukchi and Beaufort Seas: Increasing importance due to changing ice conditions?, Deep-Sea Res. Pt. II, 52, 3281-3302, https://doi.org/10.1016/j.dsr2.2005.10.006, 2005.

Elverhøi, A., Pfirman, S. L., Solheim, A., and Larssen, B. B.: Glaciomarine sedimentation in epicontinental seas exemplified by the northern Barents Sea, Mar. Geol., 85, 225-250, https://doi.org/https://doi.org/10.1016/0025-3227(89)90155-2, 1989.

Fagel, N., Not, C., Gueibe, J., Mattielli, N., and Bazhenova, E.: Late Quaternary evolution of sediment provenances in the Central Arctic Ocean: mineral assemblage, trace element composition and Nd and Pb isotope fingerprints of detrital fraction from the Northern Mendeleev Ridge, Quat. Sci. Revs., 92, 140-154, http://dx.doi.org/10.1016/j.quascirev.2013.12.011, 2014.

Fedo, C. M., Sircombe, K. N., and Rainbird, R. H.: Detrital zircon analysis of the sedimentary record, Rev. Mineral. Geochem., 53, 277-303, https://doi.org/10.2113/0530277, 2003.

Feng, H., Yao, Z., Shi, X., Zhang, Z., Lu, H., Zhang, H., Liu, Y., Shan, X., Dong, J., Dong, L., Yang, G., Hu, L., Vasilenko, Y., Astakhov, A., and Bosin, A.: Arctic zircon U-Pb ages reveal multiphase glaciations in East Siberia during the late Quaternary, Nat. Commun., 16, 7511, https://doi.org/10.1038/s41467-025-62499-y, 2025.

Gamboa, A., Montero-Serrano, J.-C., St-Onge, G., Rochon, A. and Desiage, P.-A.: Mineralogical, geochemical and magnetic signatures of surface sediments from the Canadian Beaufort Shelf and Amundsen Gulf (Canadian Arctic), Geochemistry, Geophysics, Geosystems, 18, https://doi.org/10.1002/2016GC006477, 2017.

Garzanti, E., Andò, S., Vezzoli, G., Lustrino, M., Boni, M., and Vermeesch, P.: Petrology of the Namib Sand Sea: Long-distance transport and compositional variability in the wind-displaced Orange Delta, Earth Sci. Rev., 112, 173-189, https://doi.org/10.1016/j.earscirev.2012.02.008, 2012.

Garzanti, E., and Andò, S.: Heavy mineral concentration in modern sands: Implications for provenance interpretation, in Heavy Minerals in Use, edited by: M. A. Mange and D. T. Wright, Elsevier, 58, 517-545, https://doi.org/10.1016/S0070-4571(07)58020-9, 2007.

Gordeev, V. V.: Fluvial sediment flux to the Arctic Ocean, Geomorphology, 80, 94-104, https://doi.org/10.1016/j.geomorph.2005.09.008, 2006.

Harrison, J. C., St-Onge, M. R., Petrov, O., Strelnikov, S., Lopatin, B., Wilson, F., Tella, S., Paul, D., Lynds, T. L., Shokalsky, S., Hults, C., Bergman, S., Jepsen, H. F., and Solli, A.: Geological map of the Arctic, Geol. Surv. Can., Ottawa, Ont., Open File, 5816, https://doi.org/10.4095/225705, 2008.

Harrison, J., St-Onge, M., Petrov, O., Strelnikov, S., Lopatin, B., Wilson, F., Tella, S., Paul, D., Lynds, T., Shokalsky, S., Hults, C., Bergman, S., Jepsen, H., and Solli, A.: Geological map of the arctic, Geological Survey of Canada, 2011.

Henderson, G. R., Barrett, B. S., Wachowicz, L. J., Mattingly, K. S., Preece, J. R., and Mote, T. L.: Local and remote atmospheric circulation drivers of Arctic change: A review, Front. Earth Sci., 9, 709024, https://doi.org/10.3389/feart.2021.709896, 2021.

Holmes, R. M., McClelland, J. W., Peterson, B. J., Shiklomanov, I. A., Shiklomanov, A. I., Zhulidov, A. V., Gordeev, V. V., and Bobrovitskaya, N. N.: A circumpolar perspective on fluvial sediment flux to the Arctic Ocean, Global Biogeochem. Cy., 16, 1098, https://doi.org/10.1029/2001GB001849, 2002.

IMBIE Team: Mass balance of the Greenland Ice Sheet from 1992 to 2018, Nature, 579, 233-239, https://doi.org/10.1038/s41586-019-1855-2, 2020.

Jacobsen, S. B. and Wasserburg, G. J.: Sm-Nd isotopic evolution of chondrites, Earth Planet. Sci. Lett., 50, 139-155, https://doi.org/https://doi.org/10.1016/0012-821X(80)90125-9, 1980.

Jakobsson, M.: Hypsometry and volume of the Arctic Ocean and its constituent seas, Geochem. Geophy. Geosy., 3, 1-18, https://doi.org/10.1029/2001GC000302, 2002.

Jang, K., Bayon, G., Vogt, C., Forwick, M., Ahn, Y., Kim, J.-H. and Nam, S.-I.: Non-linear response of glacier melting to Holocene warming in Svalbard recorded by sedimentary iron (oxyhydr)oxides, Earth and Planet. Sc. Lett., 607, 118054, https://doi.org/10.1016/j.epsl.2023.118054, 2023.

Kingsbury, C. G., Kamo, S. L., Ernst, R. E., Söderlund, U., and Cousens, B. L.: U-Pb geochronology of the plumbing system associated with the Late Cretaceous Strand

Fiord Formation, Axel Heiberg Island, Canada: Part of the 130-90 Ma High Arctic large igneous province, J. Geodyn., 118, 106-117, https://doi.org/10.1016/j.jog.2017.11.001, 2018.

Li, Q., Qiao, S., Shi, X., Chen, Y., Astakhov, A., Zhang, H., Hu, L., Yang, G., Bosin, A., Vasilenko, Y., and Dong, L.: Sr, Nd, and Pb isotope provenance of surface sediments on the East Siberian Arctic Shelf and implications for transport pathways, Chem. Geol., 618, 121277, https://doi.org/10.1016/j.chemgeo.2022.121277, 2023.

Li, Q., Qiao, S., Shi, X., Hu, L., Bai, Y., Zhu, A., and Cui, J.: Sediment provenance of the East Siberian Arctic Shelf: Evidence from clay minerals and chemical elements (in Chinese), Acta Oceanol. Sin., 43, 76-89, https://doi.org/10.12284/hyxb2021041, 2021.

Maccali, J., Hillaire-Marcel, C., and Not, C.: Radiogenic isotope (Nd, Pb, Sr) signatures of surface and sea ice-transported sediments from the Arctic Ocean under the present interglacial conditions, Polar Res., 37, 1442982, https://doi.org/10.1080/17518369.2018.1442982, 2018.

Martens, J., Romankevich, E., Semiletov, I., Wild, B., van Dongen, B., Vonk, J., Tesi, T., Shakhova, N., Dudarev, O. V., Kosmach, D., Vetrov, A., Lobkovsky, L., Belyaev, N., Macdonald, R. W., Pieńkowski, A. J., Eglinton, T. I., Haghipour, N., Dahle, S., Carroll, M. L., åström, E. K. L., Grebmeier, J. M., Cooper, L. W., Possnert, G., and Gustafsson, Ö.: Cascade-The circum-Arctic sediment carbon database, Earth Syst. Sci. Data, 13, 2561-2572, https://doi.org/10.5194/essd-13-2561-2021, 2021.

Martinez, N. C., Murray, R. W., Dickens, G. R., and Kölling, M.: Discrimination of sources of terrigenous sediment deposited in the central Arctic Ocean through the Cenozoic, Paleoceanography, 24, PA1210, https://doi.org/10.1029/2007PA001567, 2009.

McCave, I. N., and Andrews, J. T.: Distinguishing current effects in sediments delivered to the ocean by ice. I. Principles, methods and examples, Quat. Sci. Rev., 212, 92-107, https://doi.org/10.1016/j.quascirev.2019.03.031, 2019.

Moecher, D. P., and Samson, S. D.: Differential zircon fertility of source terranes and natural bias in the detrital zircon record: Implications for sedimentary provenance analysis, Earth Planet. Sci. Lett., 247, 252-266, https://doi.org/10.1016/j.epsl.2006.04.035, 2006.

Myers, W. B., and Darby, D. A.: A compilation of the silt and clay mineralogy from coastal and shelf regions of the Arctic Ocean, Mar. Geol., 454, 106948, https://doi.org/10.1016/j.margeo.2022.106948, 2022.

Naidu, A. S., and Mowatt, T. C.: Sources and dispersal patterns of clay minerals in surface sediments from the continental-shelf areas off Alaska, Geol. Soc. Am. Bull., 94, 841-854, https://doi.org/10.1130/0016-7606(1983)94%3C841:SADPOC%3E2.0.CO;2, 1983.

Natali, S. M., Holdren, J. P., Rogers, B. M., Treharne, R., Duffy, P. B., Pomerance, R., and MacDonald, E.: Permafrost carbon feedbacks threaten global climate goals, Proc. Natl. Acad. Sci. U.S.A., 118, e2100163118, https://doi.org/10.1073/pnas.2100163118, 2021.

Parfenov, L. M., Badarch, G., Berzin, N. A., Khanchuk, A. I., Kuzmin, M. I., Nokleberg, W. J., Prokopiev, A. V., Ogasawara, M., and Yan, H.: Summary of Northeast Asia geodynamics and tectonics, Stephan Mueller Spec. Publ. Ser., 4, 11-33, https://doi.org/10.5194/smsps-4-11-2009, 2009.

Pease, V., and Coakley, B.: Circum-Arctic Lithosphere Evolution, Geol. Soc. London Spec. Publ., 460, https://doi.org/10.1144/SP460, 2018.

Phillips, R. L., and Grantz, A.: Regional variations in provenance and abundance of ice-rafted clasts in Arctic Ocean sediments: implications for the configuration of late Quaternary oceanic and atmospheric circulation in the Arctic, Mar. Geol., 172, 91-115, https://doi.org/10.1016/S0025-3227(00)00101-8, 2001.

Puchkov, V. N., and Ivanov, K. S.: Tectonics of the Northern Urals and Western Siberia: General history of development, Geotectonics, 54, 35-53, https://doi.org/10.1134/S0016852120010100, 2020.

Rantanen, M., Karpechko, A. Y., Lipponen, A., Nordling, K., Hyvärinen, O., Ruosteenoja, K., Vihma, T., and Laaksonen, A.: The Arctic has warmed nearly four times faster than the globe since 1979, Commun. Earth Environ., 3, 168, https://doi.org/10.1038/s43247-022-00498-3, 2022.

Rino, S., Komiya, T., Windley, B. F., Katayama, I., Motoki, A., and Hirata, T.: Major episodic increases of continental crustal growth determined from zircon ages of river sands; implications for mantle overturns in the Early Precambrian, Phys. Earth Planet. Inter., 146, 369-394, https://doi.org/10.1016/j.pepi.2003.09.024, 2004.

Rossak, B. T., Kassens, H., Lange, H., Thiede, J.: Clay mineral distribution in surface sediments of the Laptev Sea: Indicator for sediments provinces, dynamics and sources, in: Land-Ocean Systems in the Siberian Arctic: Dynamics and History, edited by: Kassens, H., Bauch, H., Dmitrenko, I., Eicken, H., Hubberten, H. W., Melles, M., Thiede, J., and Timokhov, L., Springer, Berlin, Heidelberg, Germany, 587-600, https://doi.org/10.1007/978-3-642-60134-7_45, 1999.

Rusakov, V. Y., Kuz'mina, T. G., and Lukmanov, R. A.: Assessment of the sediment budget of the Kara and Laptev seas, Cont. Shelf Res., 292, 105506, https://doi.org/10.1016/j.csr.2025.105506, 2025.

Safonova, I., Maruyama, S., Hirata, T., Kon, Y., and Rino, S.: LA ICP MS U-Pb ages of detrital zircons from Russia largest rivers: Implications for major granitoid events in Eurasia and global episodes of supercontinent formation, J. Geodyn., 50, 134-153, https://doi.org/10.1016/j.jog.2010.02.008, 2010.

Saukel, C., Stein, R., Vogt, C., and Shevchenko, V. P.: Clay-mineral and grain-size distributions in surface sediments of the White Sea (Arctic Ocean): indicators of sediment sources and transport processes, Geo-Mar. Lett, 30, 605-616, https://doi.org/10.1007/s00367-010-0210-2, 2010.

Schlitzer, R.: Ocean Data View (version 5.6.2) [Software], https://hdl.handle.net/10013/epic.07f8e9e9-6111-47e9-a6dd-494af6f01c7b, 2022.

Schoster, F., Behrends, M., Müller, C., Stein, R. and Wahsner, M.: Modern river discharge in the Eurasian Arctic Ocean: Evidence from mineral assemblages and major and minor element distributions. Int. J. Earth Sci., 89, 486-495, 2000.

Screen, J. A., and Simmonds, I.: The central role of diminishing sea ice in recent Arctic temperature amplification, Nature, 464, 1334-1337, https://doi.org/10.1038/nature09051, 2010.

Serreze, M. C., and Barry, R. G.: Processes and impacts of Arctic amplification: A research synthesis, Glob. Planet. Change, 77, 85-96, https://doi.org/10.1016/j.gloplacha.2011.03.004, 2011.

Shi, F., Shi, X., Su, X., Fang, X., Wu, Y., Cheng, Z., and Yao, Z.: Clay minerals in Arctic Kongsfjorden surface sediments and their implications on provenance and paleoenvironmental change, Acta Oceanol. Sin., 37, 29-38, https://doi.org/10.1007/s13131-018-1220-6, 2018.

Stein, R., Dittmers, K. , Fahl, K., Kraus, M., Matthiessen, J., Niessen, F., Pirrung, M., Polyakova, Ye., Schoster, F., Steinke, T., and Fütterer, D.K.: Arctic (Palaeo) River Discharge and Environmental Change: Evidence from Holocene Kara Sea Sedimentary Records, Quat. Sci. Rev., 23, 1485-1511, https://doi.org/10.1016/j.quascirev.2003.12.004, 2004.

Stein, R., Frederichs, T., Fahl, K., Geibert, W., and Jansen, E.: A 430 kyr record of ice-sheet dynamics and organic-carbon burial in the central Eurasian Arctic Ocean, Nat. Commun., 16, 3822, https://doi.org/10.1038/s41467-025-59112-7, 2025.

Stein, R., Grobe, H., Wahsner, M., 1994. Organic carbon, carbonate, and clay mineral distributions in eastern central Arctic Ocean surface sediments, Mar. Geol., 119, 269-285, https://doi.org/10.1016/0025-3227(94)90185-6, 1994.

Stein, R., Matthiessen, J., Niessen, F., Krylov, R., Nam, S., and Bazhenova, E.: Towards a better (Litho-) Stratigraphy and Reconstruction of Quaternary Paleoenvironment in the Amerasian Basin (Arctic Ocean), Polarforschung, 79, 97-121, https://epic.awi.de/id/eprint/22435/1/Ste2010b.pdf, 2010.

Stein, R.: Arctic Ocean Sediments: Processes, Proxies, and Paleoenvironment, Elsevier, Amsterdam, Netherlands, 1-592, ISBN 9780444520180, 2008.

Stein, R.: Clay minerals in Arctic Ocean surface sediments [dataset]. PANGAEA, https://doi.org/10.1594/PANGAEA.992954, 2026a.

Stein, R.: Heavy minerals in Arctic Ocean surface sediments [dataset]. PANGAEA, https://doi.org/10.1594/PANGAEA.992955, 2026b.

Stevenard, N., Montero-Serrano, J.-C., Eynaud, F., St-Onge, G., Zaragosi, S., and Copland, L.: Lateglacial and Holocene sedimentary dynamics in northwestern Baffin Bay as recorded in sediment cores from Cape Norton Shaw Inlet (Nunavut, Canada), Boreas, 51, 532-552, https://doi.org/10.1111/bor.12575, 2022.

Stroeve, J., and Notz, D.: Changing state of Arctic sea ice across all seasons, Environ. Res. Lett., 15, 103001, https://doi.org/10.1088/1748-9326/aade56, 2018.

Thiry, M.: Palaeoclimatic interpretation of clay minerals in marine deposits: an outlook from the continental origin, Earth Sci. Rev., 49, 201-221, https://doi.org/10.1016/S0012-8252(99)00054-9, 2000.

Timmermans, M.-L., and Marshall, J.: Understanding Arctic Ocean Circulation: A Review of Ocean Dynamics in a Changing Climate, J. Geophys. Res. Oceans, 125, e2018JC014378, https://doi.org/10.1029/2018JC014378, 2020.

Toro, J., Miller, E. L., Prokopiev, A. V., Zhang, X., and Veselovskiy, R.: Mesozoic orogens of the Arctic from Novaya Zemlya to Alaska, J. Geol. Soc., 173, 989-1006, https://doi.org/10.1144/jgs2016-083, 2016.

Tripati, A. and Darby, D.: Evidence for ephemeral middle Eocene to early Oligocene Greenland glacial ice and pan-Arctic sea ice, Nat. Commun., 9, 1038, https://doi.org/10.1038/s41467-018-03180-5, 2018.

Troupin, C., Barth, A., Sirjacobs, D., Ouberdous, C. M., Brankart, J.-M., Brasseur, D., Rixen, M., Alvera-Azcárate, A., Belounis, M., Capet, A., Lenartz, F., Toussaint, M.-E., and Beckers, J.-M.: Generation of analysis and consistent error fields using the Data Interpolating Variational Analysis (DIVA), Ocean Model., 52–53, 90–101, https://doi.org/10.1016/j.ocemod.2012.05.002, 2012.

Tütken, T., Eisenhauer, A., Wiegand, B., and Hansen, B. T.: Glacial-interglacial cycles in Sr and Nd isotopic composition of Arctic marine sediments, Mar. Geol., 182, 351-372, https://doi.org/10.1016/S0025-3227(01)00248-1, 2002.

Vermeesch, P.: On the visualization of detrital age distributions, Chem. Geol., 312-313, 190-194, https://doi.org/10.1016/j.chemgeo.2012.04.021, 2012.

Viscosi-Shirley, C., Mammone, K., Pisias, N. G., and Dymond, J. R.: Clay mineralogy and multi-element chemistry of surface sediments on the Siberian-Arctic shelf:

implications for sediment provenance and grain size sorting, Cont. Shelf Res., 23, 1175-1200, https://doi.org/10.1016/S0278-4343(03)00091-8, 2003a.

Viscosi-Shirley, C., Pisias, N., and Mammone, K.: Sediment source strength, transport pathways and accumulation patterns on the Siberian-Arctic's Chukchi and Laptev shelves. Cont. Shelf Res., 23, 1201-1225, https://doi.org/10.1016/S0278-4343(03)00090-6, 2003b.

Vogt, C., and Knies, J.: Sediment pathways in the western Barents Sea inferred from clay mineral assemblages in surface sediments, Nor. J. Geol., 89, 41-55, https://doi.org/10.1594/PANGAEA.853649%3E, 2009.

Vogt, C.: Bulk mineralogy in surface sediments from the eastern central Arctic Ocean, Ber. Polarforsch., 212, 159-171, https://hdl.handle.net/10013/epic.10213.d001, 1996.

Vogt, C.: Regional and temporal variations of mineral assemblages in Arctic Ocean sediments as climatic indicator during glacial/interglacial changes, Ph.D. thesis, Fachbereich Geowissenschaften, University of Bremen, Bremerhaven, Germany, 309 pp., 1997.

Wahsner, M., Müller, C., Stein, R., Ivanov, G. I., Levitan, M. A., Shelekhova, E. S., and Tarasov, G. A.: Clay-mineral distribution in surface sediments of the Eurasian Arctic Ocean and continental margin as indicator for source areas and transport pathways-a synthesis, Boreas, 28, 215-233, https://doi.org/10.1111/j.1502-3885.1999.tb00216.x, 1999.

Wang, C. Y., Campbell, I. H., Stepanov, A. S., Allen, C. M., and Burtsev, I. N.: Growth rate of the preserved continental crust: II. Constraints from Hf and O isotopes in detrital zircons from Greater Russian Rivers, Geochimi. Cosmochim. Ac., 75, 1308-1345, https://doi.org/10.1016/j.gca.2010.12.010, 2011.

Wang, K., Shi, X., Dong, J., Bosin, A. A., Astakhov, A. S., and Yao, Z.: Sediment provenance of the East Siberian Arctic Shelf and evidence of Holocene climate-driven fluvial events in the Indigirka River based on detrital mineral analysis, Palaeogeog. Palaeoclimatol. Palaeoecol., 638, 112042, https://doi.org/10.1016/j.palaeo.2024.112042, 2024.

Wang, K., Shi, X., Yao, Z., Bosin, A. A., and Hu, L.: Sediment sources and transport pathways on shelves of the Chukchi and East Siberian Seas: Evidence from the heavy minerals and garnet geochemistry, Polar Sci., 33, 100873, https://doi.org/10.1016/j.polar.2022.100873, 2022.

White, D., Hinzman, L., Alessa, L., Cassano, J., Chambers, M., Falkner, K., Francis, J., Gutowski, W. J., Jr., Holland, M., Holmes, R. M., Huntington, H., Kane, D., Kliskey, A., Lee, C., McClelland, J., Peterson, B., Rupp, T. S., Straneo, F., Steele, M., Woodgate, R., Yang, D., Yoshikawa, K., and Zhang, T.: The arctic freshwater system: Changes and impacts, J. Geophys. Res. Biogeosci., 112, G04S54, https://doi.org/10.1029/2006JG000353, 2007.

White, W. M.: Geochemistry, John Wiley and Sons, Hoboken, NJ, USA, 960 pp., ISBN 9780470656679, 2013.

Yao, Z., Feng, H., Stein, R., Liu, Y., Shi, X., Vasilenko, Y., Nam, S.-I., Dong, L., Shi, F., Wang, K., Chen, Z., Qiao, S., Li, Q., Zhao, S., Pei, X., Guo, H., and Liu, Y.: Clay and detrital minerals, Sr-Nd isotopes, and zircon U-Pb ages in Arctic Ocean surface sediments – Circum-Arctic Sediment PROvenance Database (CASPROD): A database of mineralogy and geochemistry for the Circum-Arctic surface sediments, Figshare [dataset], https://doi.org/10.6084/m9.figshare.31926927, 2026.